Solar photo-ozonation: a novel treatment method for the degradation of water pollutants

Ana M. Chávez, Ana Rey, Fernando J. Beltrán, Pedro M. Álvarez*

Departamento de Ingeniería Química y Química Física. Universidad de Extremadura. Avenida de Elvas S/N, 06071 Badajoz, Spain

ABSTRACT

The decomposition of aqueous ozone by UV-visible radiation has been investigated with focus on the impact of ozone photolysis on the degradation of water pollutants during solar ozonation processes. The apparent first-order rate constants of the decomposition of ozone (k_{obs}) have been determined at various pHs in the 4-9 range using radiation of different wavelengths in the UV-visible range. It was found that UVA-visible radiation (λ>320 nm) highly enhanced ozone decomposition, especially at pH 4, for which k_{obs} was three-folded with respect to the process in the absence of radiation. Hydrogen peroxide was identified as a main intermediate of ozone photo-decomposition at pH 4. Experiments of degradation of oxalic acid by ozone showed that solar irradiation brings about an increase in the hydroxyl radical to ozone exposures ratio (R_{ct}). Finally, photo-ozonation (λ>300 nm) was shown advantageous over single ozonation in the mineralization of a selection of emerging contaminants (metoprolol, ibuprofen, N,N-diethyl-meta-toluamide and clofibric acid) in both ultrapure water and a synthetic secondary effluent. Thus, TOC removal in 2-h treatments increased from 10-25% in the absence of radiation to about 50% in the presence of radiation.

Keywords: AOP, emerging contaminants, photo-ozonation, UVA-visible radiation, water treatment

***Corresponding author:** Pedro M. Álvarez

E-mail: pmalvare@unex.es; Phone: +34 924289782; Fax: +34 924289385

1. Introduction

Ozone has been extensively used in water treatment since long due to its great oxidizing power (2.1 eV) which enables it to selectively oxidize many organic and inorganic species in aqueous solution. The reactions between ozone and organic compounds, however, usually lead to the formation of intermediates, many of which are recalcitrant to the ozone attack and, therefore, accumulate in water. In some advanced oxidation processes (AOPs), aqueous ozone can be transformed into free-radical oxygen species (ROS), such as the hydroxyl radical (HO·) which exhibits an oxidizing power (2.8 eV) even higher than that of the ozone molecule. As a consequence, these AOPs are preferred over single ozonation when the goal is to clean water avoiding the accumulation of refractory intermediates [1].

Much research has been devoted to study methods to effectively decompose ozone in water leading to the formation of ROS in order to improve oxidation efficiency. Methods to decompose aqueous ozone in alkaline solution and/or in the presence of hydrogen peroxide or UV radiation are well known [2]. In addition to those classical methods, the use of different catalysts in combination with ozone in the presence or absence of UV-vis radiation has attracted a great deal of research interest. Thus, it has been found that the transformation of aqueous ozone into hydroxyl radicals is accelerated by materials such as activated carbon, carbon nanotubes, alumina or zeolites amongst others [3-6]. Also, the combination of ozone, UV-vis radiation and some catalysts destroys organic compounds by photosensitized oxidation involving ROS [7]. Both, catalytic and photocatalytic ozonation have been proven as efficient methods to deal with water contaminants of special concern, such as emerging contaminants (ECs). Particularly, photocatalytic ozonation is a technology where synergistic effects of a number of oxidation pathways that take place simultaneously are observed [8]. However, photocatalytic ozonation is regarded as an expensive treatment technology so its applications at full-scale are scarce [7]. To overcome this drawback, solar photocatalytic ozonation has recently been investigated as a cost-effective method where the operating cost of UV lamps can be partly avoided by the use of sunlight as radiation source [9,10]. One of the first steps of the solar photocatalytic ozonation mechanism is the photolysis of ozone under solar illumination [8]. According to previous works, this step might highly contribute to the overall degradation of water pollutants. Thus, for example, it has been found that solar irradiation of a mixture of ECs (acetaminophen, antipyrine, bisphenol A, caffeine, metoprolol and testosterone) while treating it by ozone greatly improved EC removal rates and the

mineralization efficiency [9]. This might likely be due to the partial decomposition of ozone under solar radiation eventually yielding hydroxyl radicals and other ROS [11]. To our knowledge, the effect of solar radiation on the kinetics and mechanism of aqueous ozone decomposition has not been fully investigated yet.

This work is focused on the study of the effect of UV-vis radiation of different wavelengths (λ> 300 nm, λ> 320 nm and λ>390 nm) on the rate of decomposition of aqueous ozone and the formation of hydrogen peroxide and hydroxyl radicals. In addition, the degradation of a mixture of ECs (metoprolol, N,N-diethyl-meta-toluamide (DEET) and clofibric acid) in ultrapure water and in a typical secondary effluent of municipal wastewater treatment plant (MWWTP) by photo-ozonation has been studied.

2. Materials and methods

2.1. Chemicals and solutions

Four ECs were used in this research: metoprolol tartrate (CAS number: 56392-17-7), ibuprofen (CAS number: 15687-27-1), N,N-Diethyl-m-toluamide (DEET, CAS number: 134-62-3) and clofibric acid (CAS number: 882-09-7). All of them (>97%) were purchased from Sigma-Aldrich Chemical Co. (Spain) and used without further purification. In addition, oxalic acid (99%) (CAS number 144-62-7) was also obtained from Sigma-Aldrich Chemical Co. and used as target compound in degradation experiments. An aqueous solution was prepared to simulate a typical secondary effluent discharged from a MWWTP. ECs were added to the solution to reach a concentration of 2 mg L^{-1} each. The composition of the solution, after addition of ECs, is given in Table 1. Total organic carbon (TOC) of the mixture was c.a. 20 mg L^{-1}. All the reagents used to obtain this synthetic aqueous solution, except ECs, were provided by Panreac (Spain).

2.2. Photo-ozonation experimental set-up.

Photo-ozonation experiments were carried out in an experimental set-up as that shown in Fig.1. It consisted of a reactor and a commercial solar simulator (Suntest CPS, Atlas). The spherical, glass-made reactor had a working volume of 0.5 L and it was provided with a gas inlet, a gas outlet and a liquid sampling port. The reactor was thermoregulated to keep temperature at 37ºC throughout the experiments. This temperature was chosen as it is the temperature actually reached inside the solar simulator with the lamp switched on. Agitation was provided by means of a magnetic device. The reactor was placed in the chamber of the

solar simulator, which was equipped with a 1500 W air-cooled Xe arc lamp. To carry out the experiments radiation was restricted to wavelengths over 300 nm (filter A), 320 nm (filter A+B) or 390 nm (filters A+C). Filter A, made of a coated quartz glass plus a window glass (Solar Standard, Atlas), was fixed on the equipment by the manufacturer to simulate outdoors solar radiation according to DIN 67501:1999. Cut-off polyester filters B (Edmund Optics) or C (Unipapel) were additionally used to provide UVA-visible or visible radiation, respectively. Table 2 shows spectral irradiances as measured with a UV-vis spectrometer (Black Comet C model, StellarNet, USA) while operating with the different filters. As can be seen in Table 2, the overall irradiance (λ=300-800 nm) was in the range 448-550 Wm^{-2}. Ozone was produced from dry oxygen in a laboratory ozone generator (Anseros COM) and the concentration of ozone in gaseous streams entering and leaving the reactor was continuously monitored by ozone analyzers (Anseros GM-OEM and Anseros GM-PRO models, respectively).

2.3. Ozone photo-decomposition experiments.

A duplicate set of ozone decomposition experiments was first carried out in batch mode. In a typical experiment, ozone was produced from a 30 L h^{-1} dry oxygen flow in a laboratory ozone generator (Anseros COM). The gas from the ozone generator, containing about 50 mg O_3 L^{-1} was bubbled through a porous plate into the reactor previously loaded with 500 mL of 10 mM phosphate-buffered organic-free water (Milli-Q Millipore system). Gaseous ozone was fed to the reactor for 30 min to saturate the water with ozone and, at the same time, remove any trace of organic matter that could further affect the ozone stability significantly. The dissolved ozone concentration after this stage was about 7 mg L^{-1}. Then, the gas flow was stopped and the lamp of the solar simulator was switched on (in blank experiments the lamp was kept off). At intervals of time, aqueous samples were withdrawn from the reactor through a dispenser and immediately analyzed for dissolved ozone concentration.

Another duplicate set of ozone decomposition experiments was carried out in semi-batch mode in order to follow the formation of hydrogen peroxide as a product of the aqueous ozone decomposition. In these experiments, a continuous stream of an oxygen-ozone mixture (30 L h^{-1} flow rate, 50 mg L^{-1} ozone concentration) was continuously supplied to the reactor, which was previously charged with 500 mL of 10 mM phosphate-buffered organic-free water (Milli-Q Millipore system). The solar simulator lamp was kept on throughout the experiment except in blank experiments for which the lamp was always off. At different times, aqueous

samples were taken from the reactor to be analyzed for dissolved ozone and hydrogen peroxide concentrations.

2.4. Oxalic acid removal experiments.

Oxalic acid was chosen as a probe compound to test the ability of solar radiation to decompose aqueous ozone into hydroxyl radicals. Photo-ozonation experiments were carried out in semi-batch mode as described above. The reactor was first loaded with an aqueous solution of oxalic acid (pH=4, initial concentration 25 mg L^{-1}) in organic-free water (Milli-Q Millipore system). The gas flow rate and the concentration of ozone in the inlet gaseous stream were set at 15 L h^{-1} and 10 mg L^{-1}, respectively. Samples from the reactor were analyzed at different reaction times for oxalic acid concentration and TOC. Also, the evolution of the pH was followed with the reaction time.

2.5. EC degradation experiments

Photo-ozonation of a mixture of ECs (metoprolol, ibuprofen, DEET and clofibric acid) both in unbuffered organic-free water (Milli-Q Millipore system) and in a synthetic aqueous effluent (see Table 1) was carried out in semi-batch mode as described above for oxalic acid removal experiments. The reactor was charged with the aqueous solution containing the mixture of ECs and subjected to ozonation (gas flow rate 20 L h^{-1}, ozone concentration in the inlet gas 10 mg L^{-1}) in the presence and absence of radiation. A blank experiment was also carried out under illumination but in the absence of ozone to account for the direct photolysis of ECs. Samples from the reactor at different reaction times were analyzed for the concentration of ECs, short-chain carboxylic acids and TOC. pH was also followed throughout the experiments.

2.6. Analytical methods

Aqueous ozone concentration was measured by the indigo method based on the decolorization of indigo trisulfonate (600 nm, pH < 4) by ozone [12]. Hydrogen peroxide was analyzed following the cobalt colorimetric method [13]. UV-vis absorbance was recorded on a spectrophotometer (Thermo Spectronic Helios α) using a 1 cm quartz cell. Measurements of pH were made with a pH-meter (Crison GLP21+). Oxalic acid and other short-chain carboxylic acids were analyzed by ion chromatography using a Metrohm apparatus (881 Compact IC Pro model) provided with an ion suppressor and a conductivity detector. A

MetroSep A Supp 5 (250 × 4.0 mm) column thermoregulated at 45ºC was used as stationary phase. Aqueous Na_2CO_3 with a gradient program from 0.6 to 14.6 mM in 50 min and 10 min post-time equilibration and a flow rate set at 0.7 mL min^{-1} was the mobile phase. Concentrations of ECs were analyzed by HPLC with a Hitachi Elite LaChrom HPLC system provided with a diode array detector (Hitachi L-2455). A Phenomenex Gemini C18 column (150 × 3 mm, 5 µm) was used as stationary phase while a mixture of acidified ultrapure water (1% vol formic acid) (A) and acetonitrile (B) was used as mobile phase. All solvents were degassed prior to the HPLC analysis. The mobile phase flow rate was set at 0.6 mL min^{-1}. The gradient program used was as follows: start at 5% B, ramp to 50% B in 15 min, hold at 50% B for 10 min, back to 5% B in 3 min and hold at 5% B for 12 min. Detection was made at 220 nm. Retention times were as follows: metoprolol (7.5 min), DEET (16.5 min), clofibric acid (18 min) and ibuprofen (22 min). TOC was analyzed with a Shimazdu apparatus (TOC-V CSH model).

3. Results and discussion

3.1. Effect of UV-vis radiation and pH on the decomposition of aqueous ozone.

Fig.2 shows, in a semi-log graph, the profiles of ozone concentration during the course of batch experiments of ozone decomposition in buffered ultrapure water (pH=4). As it can be seen, the presence of visible radiation (λ> 390 nm) did not accelerate the decomposition of ozone with respect to that that took place in the darkness (no radiation). However, the application of radiation belonging to the entire solar spectrum (λ> 300 nm) highly increased the ozone decomposition rate. Moreover, such acceleration was mainly due to UVA radiation (λ= 320-390 nm) as deduced from Fig. 2. However, it is worth noticing that the irradiance produced by the lamp of the solar simulator in the 300-320 nm wavelength range was very limited (0.1 W m^{-2} when only filter A was used, see Table 2), which may explain the little effect observed when applying this type of radiation.

Fig.3 shows the absorption spectrum of aqueous ozone (pH=4) in the 300-800 nm wavelength range. As it can be seen, the absorption of radiation greatly increases from 340 to 300 nm while absorption above 340 nm is low. Accordingly, UV radiation in the 300-340 nm range may be pointed out as responsible for the activation of ozone decomposition. This would be likely due to the combined effect of ozone decomposition processes leading to the

formation of O(^{1}D) and, possibly, O(^{3}P), which would rapidly react with water to yield hydroxyl radicals (HO·) [14]:

$$O_3 \xrightarrow{h\nu(\lambda<310nm)} O(^1D) + O_2(a_1\Delta_g) \quad (1)$$

$$O_3 \xrightarrow{h\nu(\lambda<411nm)} O(^1D) + O_2(X^3\textstyle\sum_g^{-1}) \quad (2)$$

$$O_3 \xrightarrow{h\nu(\lambda<1180nm)} O(^3P) + O_2(a_1\Delta_g) \quad (3)$$

$$O(^1D) + H_2O \longrightarrow 2HO\cdot \quad (4)$$

$$O(^3P) + H_2O \longrightarrow 2HO\cdot \quad (5)$$

Once HO· is formed through reactions (4) and (5), decomposition of ozone is accelerated by a series of well-known reactions leading to the formation of hydrogen peroxide and ROS, such as the superoxide ion radical ($\cdot O_2^-$) and the ozonide ion radical ($\cdot O_3^-$) [15].

To quantitatively evaluate the effect of the UV-vis radiation on the ozone decomposition rate, the first-order kinetic approach was considered. Accordingly, the observed rate coefficient of ozone decay (k_{obs}) was obtained from the slope of plots such as those shown in Fig.2. Table 3 presents the values of k_{obs} for the decomposition of ozone under different conditions of radiation and pH of the aqueous solution. In all cases R^2>0.93 was found, which makes valid the assumption of first-order kinetics. As can be seen in Table 3, in the absence of radiation k_{obs} greatly increased with pH from 0.021 min^{-1} (pH 4) to 0.940 min^{-1} (pH 9). This pH effect has been extensively reported in the literature [16] and it is attributed to the initiation reaction (6) where hydrogen peroxide in its anionic form (HO_2^-) is generated. This triggers the decomposition of ozone through a radical-chain mechanism where a number of ROS such as HO·, $\cdot O_2H/\cdot O_2^-$ and $\cdot O_3H/\cdot O_3^-$ are involved [15]:

$$O_3 + OH^- \xrightarrow{k=70M^{-1}s^{-1}} HO_2^- + O_2 \quad (6)$$

The effect of radiation on the rate of aqueous ozone decomposition was strong at pH 4. Thus, in the presence of radiation of λ> 300 nm (see Table 1 for irradiance distribution) k_{obs} was four folded compared to the value achieved in the absence of any radiation. At pH 7 and 9 the effect of radiation was of less significance (k_{obs} increased by factors of 1.5 and 1.2 at pH 7 and 9, respectively).This result suggests that at neutral and alkaline conditions, reaction (6) is the main initiation step, which hinders the contributions of reactions (1) to (5). At pH<7,

however, the contribution of ozone photolysis to the initiation of the radical-chain mechanism of ozone decomposition must be taken into consideration.

3.2. Hydrogen peroxide as intermediate of ozone decomposition

Hydrogen peroxide is an initiator and promoter of the aqueous ozone decomposition as it can react with both ozone and HO· to form other ROS such as the pairs $\cdot O_2H/\cdot O_2^-$ and $\cdot O_3H/\cdot O_3^-$, which accelerate the transformation of ozone into HO·. Fig 4 shows the concentration of hydrogen peroxide during the course of some semi-batch ozone decomposition experiments. From Fig 4 it is apparent that, at pH 4, the net formation of hydrogen peroxide during ozone decomposition is favored by radiation (λ< 300 nm), suggesting that, at this condition, hydrogen peroxide is an intermediate of reactions (4) and (5). At higher pH (i.e., pH 7 and 9), however, the profiles of hydrogen peroxide concentration were quite similar both in the presence and absence of radiation. Although formation of hydrogen peroxide at high pH might be also enhanced by radiation, it could not accumulate in solution to a high degree because it would rapidly react with ozone and HO· mainly through reactions (7) and (8) [15]:

$$O_3 + HO_2^- \xrightarrow{k=2.2\times10^6\ M^{-1}s^{-1}} \cdot O_3^- + \cdot O_2H \quad (7)$$

$$HO\cdot + HO_2^- \xrightarrow{k=7.5\times10^9\ M^{-1}s^{-1}} \cdot O_2^- + H_2O \quad (8)$$

To further explore the effect of radiation on the net formation of hydrogen peroxide during decomposition of ozone at pH 4, a new set of semi-batch experiments was carried out applying radiation of different wavelength ranges. Fig. 5 shows the concentration profiles of hydrogen peroxide during the course of these experiments. It can be observed that hydrogen peroxide concentration in solution increased fast from the beginning of any experiment. However, the initial rate of hydrogen peroxide formation depended on the type of radiation applied. Thus, when radiation λ>300 nm or λ>320 nm was used, hydrogen peroxide concentration reached concentrations of c.a. 9×10^{-6} M in about 30 min while when only visible radiation was applied (λ>390 nm) half that concentration was analyzed in water after 30 min. In the blank experiment, carried out without radiation, the concentration of hydrogen peroxide was even lower (< 2×10^{-6} M after 30 min). If Fig 2 and Fig 5 are analyzed together, it can be easily deduced that the use of radiation accelerates both ozone decomposition and hydrogen peroxide generation following the same trend. This result suggests that, at pH 4, the

generated hydrogen peroxide may play an important role on ozone decomposition, especially at wavelengths in the 300-390 nm range. At λ>390 nm, hydrogen peroxide, though formed to some extent, is not expected to undergo photolysis and, therefore, accelerate ozone transformation into ROS. In accordance with this, Chu and Anastasio [17] found that the absorption coefficient of aqueous hydrogen peroxide at slightly acidic conditions decreased with the increasing wavelength from c.a. 1 $M^{-1}\cdot cm^{-1}$ at 300 nm to nearly 0 at 360 nm. Therefore, it is plausible to consider that hydrogen peroxide is a primary intermediate of ozone decomposition that may further decompose into ROS both by radiation (λ< 360 nm) and by the well-known mechanism of ozone decomposition in water [9].

3.3. Kinetic model for aqueous ozone decomposition at pH 4 under illumination

An attempt to model the kinetics of aqueous ozone decomposition under illumination was carried out. Considering the findings above, reactions (9) and (10) were assumed as main photolytic steps:

$$O_3 \xrightarrow{h\nu} O_2 + H_2O_2 \quad (9)$$

$$H_2O_2 \xrightarrow{h\nu} 2HO\cdot \quad (10)$$

In addition, reactions in Table 4 were considered to develop a mathematical model aimed to simulate the kinetics of ozone decay in batch experiments. Rate constant data in Table 4 were taken or adapted from the literature [18-20]. The mathematical model, which considers a set of differential equations for ozone, hydrogen peroxide and free-radical species, was numerically solved by a fourth-order Runge-Kutta method (Micromath Sicentist 3.0) to obtain the ozone concentration profile. The values of the rate constants of reactions (9) and (10) were found matching the experimental profiles of ozone concentration and the simulated ones. Fig. 6 shows the actual ozone concentration profiles and those simulated for experiments in the absence and presence of radiation. As can be seen, good agreement (R^2 > 0.99) was observed between the experimental and calculated values, which validates the model used. Therefore, the computational method allowed the estimation of the rate constants of reactions (7) and (8) as shown in Table 5. As expected, both rate constants were much lower for λ>390 nm than for λ>300 nm or λ>320 nm.

3.4. Effect of radiation on the degradation of oxalic acid by ozonation: R_{ct} ratios

Oxalic acid was chosen as a probe compound to test the ability of UV-vis radiation (λ>300 nm) to decompose aqueous ozone into ROS, mainly hydroxyl radical. Aqueous oxalic acid (pH 4) does not absorb radiation of λ>300 nm as it was deduced from the absorption spectrum acquired (results not shown). Also, oxalic acid reacts very slowly with molecular ozone ($k<0.04\ M^{-1}\cdot s^{-1}$ at pH=4 as obtained from [21]) while does react fast with the hydroxyl radical ($k= 2.3x10^7\ M^{-1}\cdot s^{-1}$ at pH=4 as obtained from [22]) leaving no intermediates in solution as it is transformed directly to CO_2. This latter is corroborated by results in Fig.7 where residual normalized concentration of oxalic acid and TOC during the course of ozonation and photo-ozonation experiments at pH 4 are plotted together. It can be seen that for given reaction conditions oxalic acid and TOC profiles are close to each other.

The effect of radiation on the removal of oxalic acid is clear from the results in Fig. 5. Thus, oxalic acid removal rate was greatly enhanced by using UV-vis radiation (λ> 300 nm or λ> 320 nm). Little differences were observed between the oxalic acid concentration profiles from photo-ozonation experiments carried out with filters A (λ> 300 nm) and A+B (λ> 320 nm). These results suggest that ozone decomposition in the presence of UV-vis radiation involves a greater generation of secondary oxidants (i.e., ROS) able to remove oxalic acid.

As the rate constants of the reaction between oxalic acid and ROS other than HO· are much lower than that reported for the reaction oxalic acid-HO· [23], one can consider that oxalic acid depletion during ozonation is primarily due to hydroxyl radical reactions. Accordingly, it can be assumed that the degradation of oxalic acid by ozonation or photo-ozonation obeys a second order kinetic law as follows:

$$-\frac{dC_{OX}}{dt} \approx k_{HO}\cdot C_{OX}\cdot C_{HO\cdot} \qquad (11)$$

In Eq. (11), C_{OX} stands for the concentration of oxalic acid, $C_{HO\cdot}$ for the concentration of hydroxyl radicals in solution and $k_{HO\cdot}$ for the second-order rate constant of the reaction between oxalic acid and hydroxyl radicals. Rearranging equation (11) and integrating:

$$\ln \frac{C_{OX,0}}{C_{OX,t}} = k_{HO\cdot} \cdot \int_0^t C_{HO\cdot} dt \quad (12)$$

This allows one to determine the ratio of exposures of HO· and ozone (R_{ct}) during ozonation experiments as follows [24]:

$$R_{ct} = \frac{C_{HO\cdot}}{C_{O_3}} = \frac{\int_0^t C_{HO\cdot} dt}{\int_0^t C_{O_3} dt} = \frac{\ln \frac{C_{OX,0}}{C_{OX,t}}}{k_{HO\cdot} \int_0^t C_{O_3} dt} \quad (13)$$

Fig. 8 shows plots of ln ($C_{OX,0}/C_{OX,t}$) versus the ozone exposure ($\int C_{O3} \cdot dt$) measured in some ozonation and photo-ozonation experiments. Fig. 8 demonstrates a strong dependence of R_{ct} on the presence of radiation (λ>300 nm). Thus, R_{ct}, which was constant throughout the experiments (R^2>0.98), took an average value of 6.2×10^{-8} for the single ozonation experiment while in the presence of radiation the HO· exposure increased dramatically leading to much higher values of R_{ct} (average values of 1.4×10^{-5} and 6.5×10^{-6} for experiments carried out with radiation λ>300 nm and λ>320 nm, respectively).

3.5. Degradation of a mixture of ECs by photo-ozonation

Finally, a set of experiments was primarily designed to elucidate the effect of solar photo-ozonation on the mineralization of organic compounds of special concern, such as ECs. For that purpose, four ECs were selected: metoprolol, ibuprofen, DEET and clofibric acid. Blank experiments (in the absence of ozone) demonstrated that none of these compounds could be removed significantly by direct photolysis at λ> 300 nm (not shown). Thus, EC removal percentages after 2-hour treatment were below 1%. Semi-batch ozonation experiments were carried out both in ultrapure water and in a synthetic effluent prepared to simulate a typical secondary effluent from a MWWTP (see Table 1). Fig. 9 shows the degradation of ECs in terms of overall removal and mineralization (i.e, TOC removal). It is apparent that single ozonation (in the absence of radiation) was able to completely remove the four ECs in less than 20 min regardless of the water matrix used. Moreover, no effect of radiation was observed on the removal rate of ECs. However, the impact of radiation on TOC removal was considerable. Thus, while single ozonation (i.e., absence of radiation) led to only about 25% TOC removal after 2 hours of ozonation of the aqueous solution of ECs (ultrapure water), 50% TOC removal was achieved by photo-ozonation. The impact of radiation on

mineralization was also evident in the experiments carried out with the synthetic effluent. Thus, while single ozonation barely removed 10% of the initial TOC in 2 h of treatment, about 45% TOC removal was achieved within this time in the photo-ozonation experiment. These results suggest that, once the ECs were transformed into ozone-refractory intermediates, radiation (λ>300 nm) promoted an ozone decomposition free-radical mechanism leading to the overall degradation of ECs and partial mineralization of the synthetic effluent. This finding could be useful to design photo-ozonation processes aimed to degrade pollutants in water which are difficult to mineralize by single ozonation.

Partial oxidation of ECs in the ozonation experiments carried out with the synthetic effluent (i.e., TOC removal was not complete) suggests the accumulation of reaction intermediates. As pH decreased from c.a. 7 to about 4.5-5 as a result of ozonation, the formation of some carboxylic acid was analyzed by ion chromatography. Oxalic acid was the main reaction intermediate though noticeable amounts of formic acid and acetic acid were also formed. Succinic and malonic acids were also detected as reaction intermediates in some instances. Fig. 10 presents the evolution with time of these carboxylic acids, considered as a whole in terms of organic carbon (TOC_{carbx}), during ozonation experiments in the presence and absence of radiation. It can be seen that the production rate of carboxylic acids was almost constant during the 2-hour single ozonation experiment while the TOC_{carbx} increased to reach a maximum at 90 min in the photo-ozonation and decreased afterwards. A TOC balance revealed that after 2 hours of treatment the residual TOC was partly due to the accumulation of carboxylic acids. Thus the TOC_{carbx}/TOC ratio at 2 h was 16.7% in the single ozonation experiment (no radiation) and 45.7% in the photo-ozonation experiment. This points out the photo-ozonation process as a more efficient one in terms of overall organic matter degradation.

4. Conclusions

In this study the experimental results show that aqueous ozone transformation into ROS can be accelerated by solar radiation (λ> 300 nm). The acceleration is higher at pH 4 than at pH 7 or 9. At pH 4 and considering other experimental conditions used in this work, ozone photo-decomposition is mainly due to radiation in the 320-390 wavelength range. Hydrogen peroxide was identified as an intermediate of ozone photo-decomposition, which eventually yield a higher concentration of hydroxyl radicals than single ozonation (in the absence of radiation). Thus, it was found that the hydroxyl radical-to-ozone exposure ratio (R_{ct}) could be

more than 100 folded by using UVA-vis radiation (λ> 320 nm). In this work it has been shown that photo-ozonation is a more efficient process than single ozonation to mineralize a mixture of four selected ECs both in aqueous solution (ultrapure water) and in a synthetic effluent prepared to simulate a secondary effluent from a MWWTP. Accordingly, solar photo-ozonation could be regarded as an efficient oxidation method of water pollutants which are difficult to mineralize.

Acknowledgements

Authors thank the Spanish MINECO and European Feder Funds (CTQ2012-35789-C02-01) for economic support. Ms Chávez is also thankful to the Spanish MINECO for her predoctoral contract (call 2013).

References

[1] R. Andreozzi, V. Caprio, A. Insola, R. Marotta, Advanced oxidation processes (AOP) for water purification and recovery, Catalysis Today, 53 (1999) 51–59.

[2] W.H. Glaze, J.W. Kang, D.H. Chapin, The chemistry of water treatment processes involving ozone, hydrogen peroxide and ultraviolet radiation, Ozone: Science & Engineering, 9 (1987) 335–352

[3] P.M. Alvárez, J.F. García-Araya, F.J. Beltrán, I. Giráldez, J. Jaramillo, V. Gómez-Serrano. The influence of various factors on aqueous ozone decomposition by granular activated carbons and the development of a mechanistic approach, Carbon, 44 (2006) 3102-3112

[4] A. Ikhlaq, D.R. Brown, B. Kasprzyk-Hordern, Mechanisms of catalytic ozonation: An investigation into superoxide ion radical and hydrogen peroxide formation during catalytic ozonation on alumina and zeolites in water, Applied Catalysis B- Environmental, 129 (2013) 437-449

[5] R. Oulton, J.P. Haase, S. Kaalberg, C.T. Redmond, M.J. Nalbandian, D.M. Cwiertny, Hydroxyl radical formation during ozonation of multiwalled carbon nanotubes: Performance optimization and demonstration of a reactive CNT filter, Environmental Science and Technology, 49 (2015) 3687-3697

[6] J. Nawrocki, L. Fijolek, Catalytic ozonation- Effect of carbon contaminants on the process of ozone decomposition, Applied Catalysis B-Environmental, 142 (2013) 307-314.

[7] M. Mehrjouei, S. Mueller, D. Moeller, A review on photocatalytic ozonation used for the treatment of water and wastewater, Chemical Engineering Journal, 263 (2015) 209-219.

[8] E. Rodríguez, G. Fernández, P.M. Álvarez, F.J. Beltrán, TiO_2 and Fe (III) photocatalytic ozonation processes of a mixture of emergent contaminants of water, Water Research, 46 (2012) 152-166.

[9] D.H. Quiñones, P.M. Álvarez, A. Rey, S. Contreras, F.J. Beltrán, Application of solar photocatalytic ozonation for the degradation of emerging contaminants in water in a pilot plant, Chemical Engineering Journal, 260 (2015) 399-410.

[10] D.H. Quiñones, D.H., P.M. Álvarez, A. Rey, F.J. Beltrán, Removal of emerging contaminants from municipal WWTP secondary effluents by solar photocatalytic ozonation. A pilot-scale study, Separation and Purification Technology, 149 (2015) 132-139.

[11] L. Sánchez, X. Doménech, J. Casado, J. Peral, Solar activated ozonation of phenol and malic acid, Chemosphere, 50 (2003) 1085-1093.

[12] H. Bader, J. Hoigné, Determination of ozone in water by the indigo method, Water Research 15 (1981) 449-456.

[13] W. Masschelein, M. Denis, R. Ledent, Spectrophotometric determination of residual hydrogen peroxide, Water Sewage Works, 124 (1997) 69-72.

[14] J.M. Anglada, M. Martins-Costa, M.F. Ruíz-López, J.S. Francisco, Spectroscopic signatures of ozone at the air-water interface and photochemistry implications, Proceedings of the National Academy of Sciences of the United States of America, 111 (2014) 11618-11623.

[15] J. Staehelin, R.E. Buhler, J. Hoigné, Ozone decomposition in water studied by pulse radiolysis. 2. OH and HO4 as chain intermediates, Journal of Physical Chemistry, 88 (1984) 5999–6004.

[16] J.L. Sotelo, F.J. Beltrán, F.J. Benítez, J. Beltrán-Heredia, Ozone decomposition in water: kinetic study, Industrial and Engineering Chemical Research, 26 (1987) 39-43.

[17] L. Chu, C. Anastasio, Formation of hydroxyl radical from the photolysis of frozen hydrogen peroxide, Journal of Physical Chemistry A, 109 (2005) 6264-6271.

[18] F.J. Beltrán, J. Rivas, P.M. Álvarez, M.A. Alonso, B. Acedo, A kinetic model for advanced oxidation processes of aromatic hydrocarbons in water: Application to phenantrene and nitrobencene, Industrial and Engineering Chemistry Research, 38 (1999) 4189–4199.

[19] J. Lin, T. Nakajima, An AM1 study of decomposition of aqueous ozone. Journal of Molecular:THEOCHEM, 625 (2003) 161–167.

[20] P. Maruthamuthu, P. Neta, Phosphate radicals, spectra, acid-base equilibria and reactions with inorganic compounds. The Journal of Physical Chemistry, 82 (1978) 710-713.

[21] J. Hoigné, H. Bader, Rate constants of reactions of ozone with organic and inorganic compounds in water – II. Dissociating organic compounds, Water Research, 17 (1983), 185-194.

[22] G.V. Buxton, C.L. Greenstock, W.P. Helman, A.B. Ross, Critical review of rate constants for reactions of hydrated electrons, hydrogen atoms and hydroxyl radicals (·OH/·O^-) in aqueous solution, Journal of Physical Chemistry, 17 (1988) 513-886.

[23] T. Garoma, M.D. Gurol, Modeling aqueous ozone/UV process using oxalic acid as probe chemical, Environmental Science and Technology, 39 (2005) 7964-7969.

[24] M.S. Elovitz, U. von Gunten, Hydroxyl radical/ozone ratios during ozonation processes. I. The R(ct) concept, Ozone: Science and Engineering, 21 (1999) 239-260.

List of tables:

Table 1. Chemical composition of the synthetic effluent used in this work

Chemical	Concentration (mg L^{-1})
Beef extract powder	3.6
Meat peptone	5.4
Humic acid	8.5
Tannic acid	8.4
Lignosulfonic acid sodium salt	4.9
Sodium lauryl sulfate	2.0
Arabic acid	9.4
Gum Arabic from acacia tree	9.4
Magnesium sulfate 7-hydrate	2.9
Ammonium sulfate	14.2
Metropolol tartrate	2.0
Ibuprofen	2.0
N,N-diethyl-meta-toluamide (DEET)	2.0
Clofibric acid	2.0

Table 2. Irradiance distribution produced by the lamp and cut-off filters used in this work

Cut-off filter	Irradiance (W m^{-2})			
	λ=300-320 nm	λ=320-390 nm	λ=390-800 nm	λ=300-800 nm
A	0.1	50.6	499.3	550.0
A+B	<0.01	40.5	469.3	509.8
A+C	< 0.01	< 1.0	447.4	448.4

17

Table 3. Apparent first-order rate constant of aqueous ozone decomposition at various pHs and irradiation wavelength ranges

Irradiation	pH=4		pH=7		pH=9	
	k_{obs} (min^{-1})	R^2	k_{obs} (min^{-1})	R^2	k_{obs} (min^{-1})	R^2
No radiation	0.021±0.001	0.978	0.181±0.005	0.967	0.940±0.066	0.996
hν (λ>390 nm)	0.020±0.001	0.974	0.259±0.012	0.910	1.181±0.090	0.947
hν (λ>320 nm)	0.066±0.002	0.985	0.272±0.010	0.976	1.030±0.018	0.938
hν (λ>300 nm)	0.084±0.002	0.990	0.273±0.012	0.974	1.152±0.100	0.935

18

19

20

Table 4. Reactions and rate constants considered in the mechanism of ozone decomposition under illumination

Reaction	Rate constant (T=37ºC)
$O_3 + OH^- \longrightarrow HO_2^- + O_2$	k= 390 $M^{-1}s^{-1}$
$O_3 + HO_2^- \longrightarrow O_3^{\bullet -} + HO_2^{\bullet}$	k= 1.09x10^7 $M^{-1}s^{-1}$
$O_3 + O_2^{\bullet -} \longrightarrow O_3^{\bullet -} + O_2$	k= 1.6x10^9 $M^{-1}s^{-1}$
$HO_3^{\bullet} \longrightarrow HO^{\bullet} + O_2$	k= 1.4x10^5 $M^{-1}s^{-1}$
$O_3 + HO^{\bullet} \longrightarrow HO_2^{\bullet} + O_2$	k= 3x10^9 $M^{-1}s^{-1}$
$H_2O_2 + HO^{\bullet} \longrightarrow HO_2^{\bullet} + H_2O$	k= 2.7x10^7 $M^{-1}s^{-1}$
$HO_2^- + HO^{\bullet} \longrightarrow O_2^{\bullet -} + H_2O$	k= 7.5x10^9 $M^{-1}s^{-1}$
$O_3 \longrightarrow O + O_2$	k= 1.69x10^{-6} s^{-1}
$O + O_2 \longrightarrow O_3$	k= 4x10^9 $M^{-1}s^{-1}$
$O + H_2O \longrightarrow 2HO^{\bullet}$	k= 2.5x10^3 s^{-1}
$H_3PO_4 + HO^{\bullet} \longrightarrow P_1$	k= 2.6x10^6 $M^{-1}s^{-1}$
$H_2PO_4^- + HO^{\bullet} \longrightarrow P_2$	k= 2.0x10^4 $M^{-1}s^{-1}$
$HPO_4^{2-} + HO^{\bullet} \longrightarrow P_3$	k= 7.9x10^5 $M^{-1}s^{-1}$
$O_3 + H_2O + h\nu \xrightarrow{H^+} 2HO^{\bullet} + H_2O_2$	$k_{O3\text{-}rad}$ s^{-1}
$H_2O_2 + h\nu \longrightarrow 2HO^{\bullet}$	$k_{H2O2\text{-}rad}$ s^{-1}
$HO_2^- + H^+ \rightleftharpoons H_2O_2$	pK= 11.3
$HO_2^{\bullet} \rightleftharpoons O_2^{\bullet -} + H^+$	pK= 4.8
$O_3^{\bullet -} + H^+ \rightleftharpoons HO_3^{\bullet}$	pK= 8.2
$H_3PO_4 \rightleftharpoons H^+ + H_2PO_4^-$	pK= 2.2
$H_2PO_4^- \rightleftharpoons H^+ + HPO_4^{2-}$	pK= 7.2
$HPO_4^{2-} \rightleftharpoons H^+ + PO_4^{3-}$	pK= 12.3

21

22

Table 5. Rate constants of photolytic decomposition of ozone and hydrogen peroxide at pH 4 according to the reactions model shown in Table 4

Radiation	$k_{O3\text{-}rad}$ (s^{-1})	$k_{H2O2\text{-}rad}$ (s^{-1})	R^2
hν (λ>390 nm)	1.01×10^{-9}	1.15×10^{-10}	0.997
hν (λ>320 nm)	1.05×10^{-7}	9.53×10^{-4}	0.993
hν (λ>300 nm)	1.13×10^{-7}	9.98×10^{-4}	0.990

23
24

Figure captions:

Fig. 1. Experimental set-up used to carry out photo-ozonation experiments. (1) Oxygen bottle, (2) ozone generator, (3) flow meter, (4) ozone analyzer (inlet stream), (5) ozone outlet analyzer (outlet stream), (6) solar simulator, (7) agitated reactor, (8) magnetic stirrer, (9) sampling port.

Fig. 2. Time-evolution of normalized aqueous ozone concentration during the course of batch ozone decomposition experiments. Experimental conditions: V=500 mL, pH=4 (10 mM phosphate buffer), $C_{O3,0}=1.5x10^{-4}$ M, T=37ºC. Symbols: ■ No radiation, ● Radiation (λ=300-800 nm), filter A ◇ Radiation (λ=320-800 nm), filter A+B, △ Radiation (λ=390-800 nm), filter A+C. See Table 2 for irradiance distribution.

Fig. 3. Absorption spectrum of aqueous ozone in the wavelength range 300-800 nm. Conditions: pH=4 (10 mM phosphate buffer), $C_{O3,0}=1.5x10^{-4}$ M.

Fig. 4. Time-evolution of hydrogen peroxide concentration during the course of semi-batch ozone absorption-decomposition experiments. Influence of pH and radiation. Experimental conditions: V=500 mL, T=37ºC, Phospate buffer = 10 mM, Ozone dosage=25 mg min^{-1}. Symbols: pH=4 [● O_3, ▲ Photo-ozonation (λ>300 nm)], pH=7 [● O_3, △ Photo-ozonation (λ>300 nm)], pH=9 [○ O_3, △ Photo-ozonation (λ>300 nm)].

Fig. 5. Time-evolution of hydrogen peroxide concentration during the course of semi-batch ozone absorption-decomposition experiments. Influence of radiation wavelength. Experimental conditions: V=500 mL, pH=4, T=37ºC, Phospate buffer = 10 mM, Ozone dosage=25 mg min^{-1}. Symbols: ● O_3, ▲ Photo-ozonation (λ>300 nm), □ Photo-ozonation (λ>320 nm), ◇ Photo-ozonation (λ>390 nm).

Fig. 6. Time-evolution of normalized aqueous ozone concentration during the course of batch ozone decomposition experiments. Experimental conditions: V=500 mL, pH=4 (10 mM phosphate buffer), $C_{O3,0}=1.5x10^{-4}$ M, T=37ºC. Symbols: ■ No radiation, ● Radiation (λ=300-800 nm), filter A ◇ Radiation (λ=320-800 nm), filter A+B, △ Radiation (λ=390-800 nm), filter A+C. See Table 2 for irradiance distribution. Solid lines represents fitting results according to the model in Table 4.

Fig. 7. Time-evolution of normalized oxalic acid concentration and normalized TOC during the course of semi-batch ozonation and photo-ozonation experiments. Experimental conditions: V=500 mL, $C_{OXAL,0}$=25 mg L^{-1}, pH_0=4, T=37ºC, Ozone dosage=2.5 mg min^{-1}. Symbols: ■, □ O_3; ●, ○ Photo-ozonation (λ>300 nm); ▲,△ Photo-ozonation (λ>320 nm). Solid symbols for oxalic acid, open symbols for TOC.

Fig. 8. R_{ct} plots for ozonation and photo-ozonation semi-batch experiments. Operating conditions: V=500 mL, $C_{OXAL,0}$=25 mg L^{-1}, pH_0=4, T=37ºC, Ozone dosage=2.5 mg min^{-1}. Symbols: ■ O_3, ● Photo-ozonation (λ>300 nm), △ Photo-ozonation (λ>320 nm).

Fig. 9. Time-evolution of normalized overall ECs concentration and normalized TOC during the course of semi-batch ozonation and photo-ozonation (λ>320 nm) experiments. Experimental conditions: V=500 mL, $C_{EC,0}$=2 mg L^{-1} each, TOC_0= 4 mg·L^{-1} (ultrapure water spiked with ECs) or 20 mg·L^{-1} (synthetic effluent), pH_0=7, T=37ºC, Ozone dosage=3.3 mg min^{-1}. Symbols: ■ □ O_3, TOC profile; ●, ○ O_3, ECs concentration profile; ◆,◇ Photo-ozonation, TOC profile; ▲,△ Photo-ozonation, ECs concentration profile. Solid symbols for experiments with the synthetic effluent (see Table 1), open symbols for experiments carried out in ultrapure water spiked with ECs.

Fig. 10. Time-evolution of short-chain carboxylic acids (measured as organic carbon) accumulated during ozonation and photo-ozonation semi-batch experiments carried out with the synthetic effluent. Experimental conditions: V=500 mL, $C_{EC,0}$=2 mg L^{-1} each TOC_0=20 mg L^{-1}, pH_0=7, C_{O3ge}=10 mg L^{-1}, Q=20 L h^{-1}, T=37ºC, Ozone dosage=3.3 mg min^{-1}. Symbols: ● O_3, ○ Photo-ozonation (λ>300 nm).

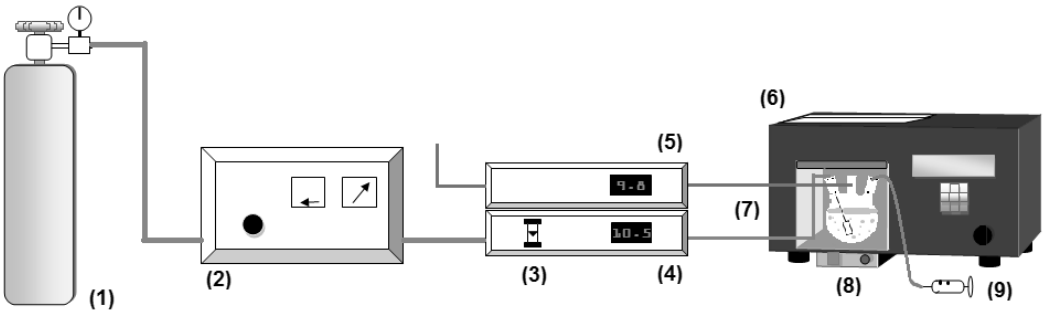

Fig. 1. Experimental set-up used to carry out photo-ozonation experiments. (1) Oxygen bottle, (2) ozone generator, (3) flow meter, (4) ozone analyzer (inlet stream), (5) ozone outlet analyzer (outlet stream), (6) solar simulator, (7) agitated reactor, (8) magnetic stirrer, (9) sampling port.

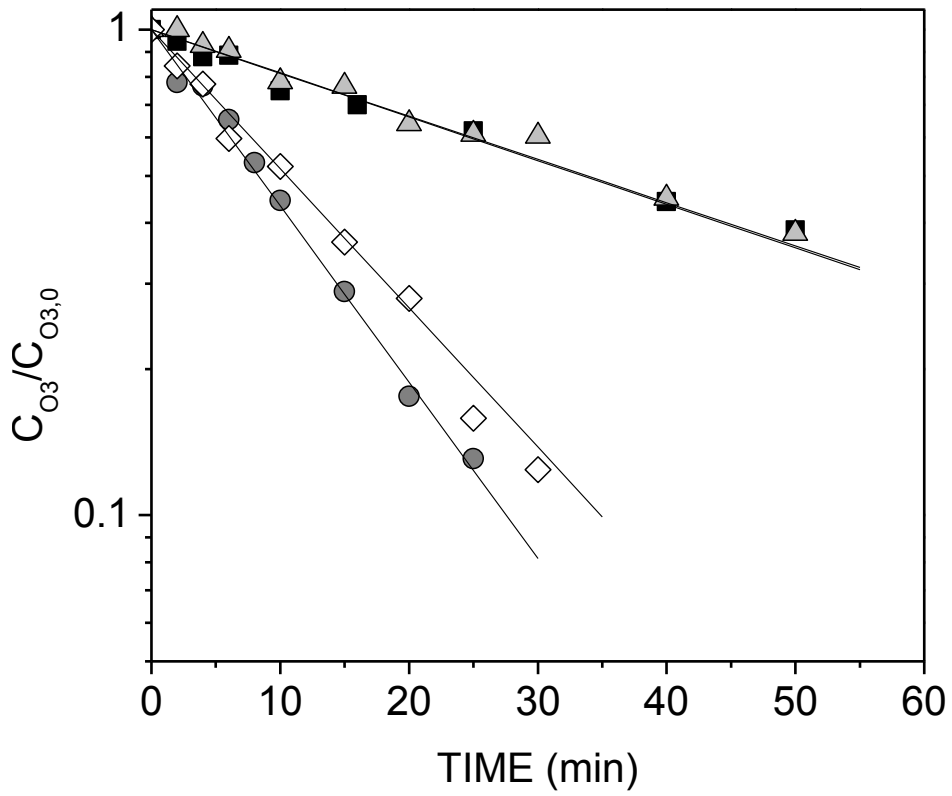

Fig. 2. Time-evolution of normalized aqueous ozone concentration during the course of batch ozone decomposition experiments. Experimental conditions: V=500 mL, pH=4 (10 mM phosphate buffer), $C_{O3,0}$=1.5x10^{-4} M, T=37ºC. Symbols: ■ No radiation, ● Radiation (λ=300-800 nm), filter A ◇ Radiation (λ=320-800 nm), filter A+B, △ Radiation (λ=390-800 nm), filter A+C. See Table 2 for irradiance distribution.

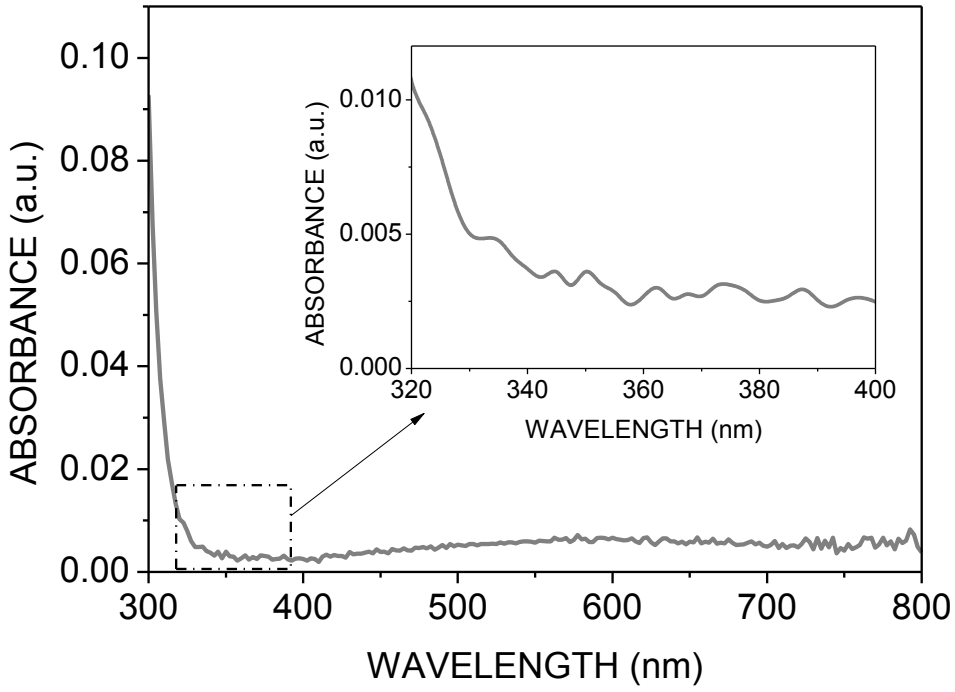

Fig. 3. Absorption spectrum of aqueous ozone in the wavelength range 300-800 nm. Conditions: pH=4 (10 mM phosphate buffer), $C_{O3,0}$=1.5x10^{-4} M.

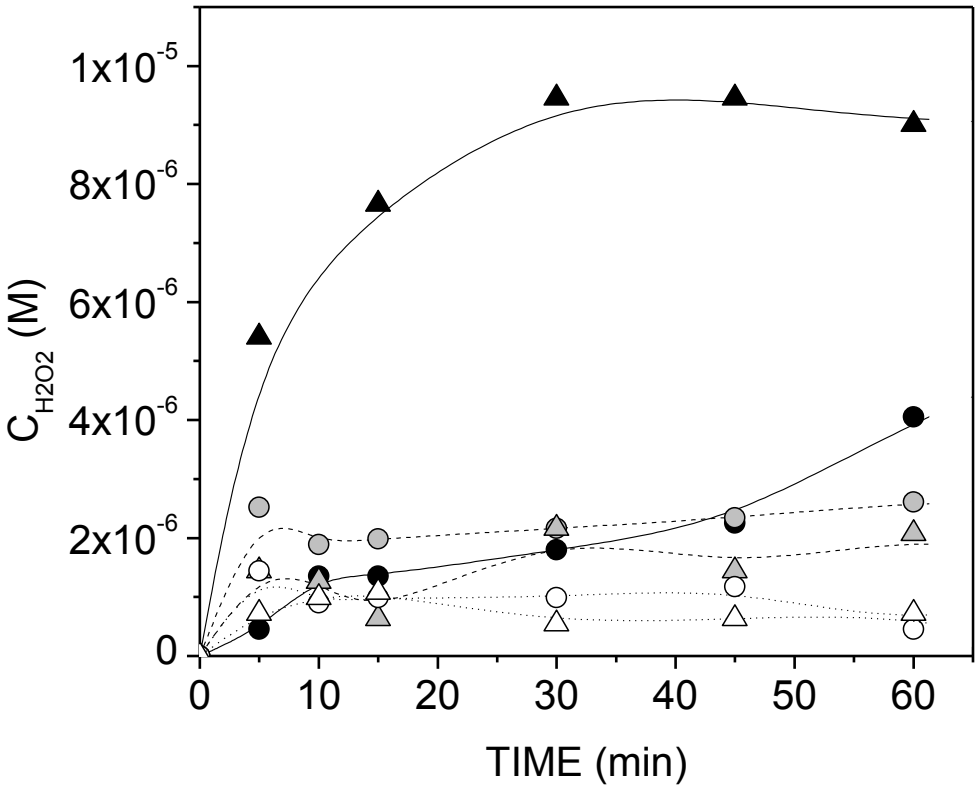

Fig. 4. Time-evolution of hydrogen peroxide concentration during the course of semi-batch ozone absorption-decomposition experiments. Influence of pH and radiation. Experimental conditions: V=500 mL, T=37ºC, Phospate buffer = 10 mM, Ozone dosage=25 mg min^{-1}. Symbols: pH=4 [● O_3, ▲ Photo-ozonation (λ>300 nm)], pH=7 [◍ O_3, ◬ Photo-ozonation (λ>300 nm)], pH=9 [○ O_3, △ Photo-ozonation (λ>300 nm)].

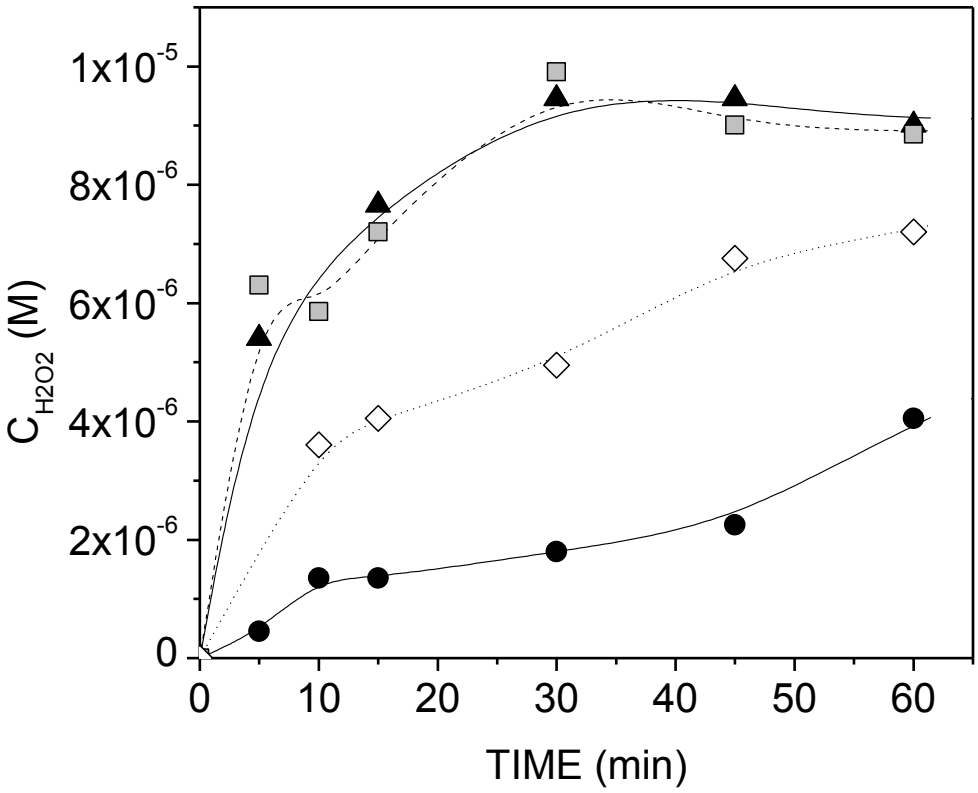

Fig. 5. Time-evolution of hydrogen peroxide concentration during the course of semi-batch ozone absorption-decomposition experiments. Influence of radiation wavelength. Experimental conditions: V=500 mL, pH=4, T=37ºC, Phospate buffer = 10 mM, Ozone dosage=25 mg min^{-1}. Symbols:● O_3, ▲ Photo-ozonation (λ>300 nm), ■ Photo-ozonation (λ>320 nm), ◇ Photo-ozonation (λ>390 nm).

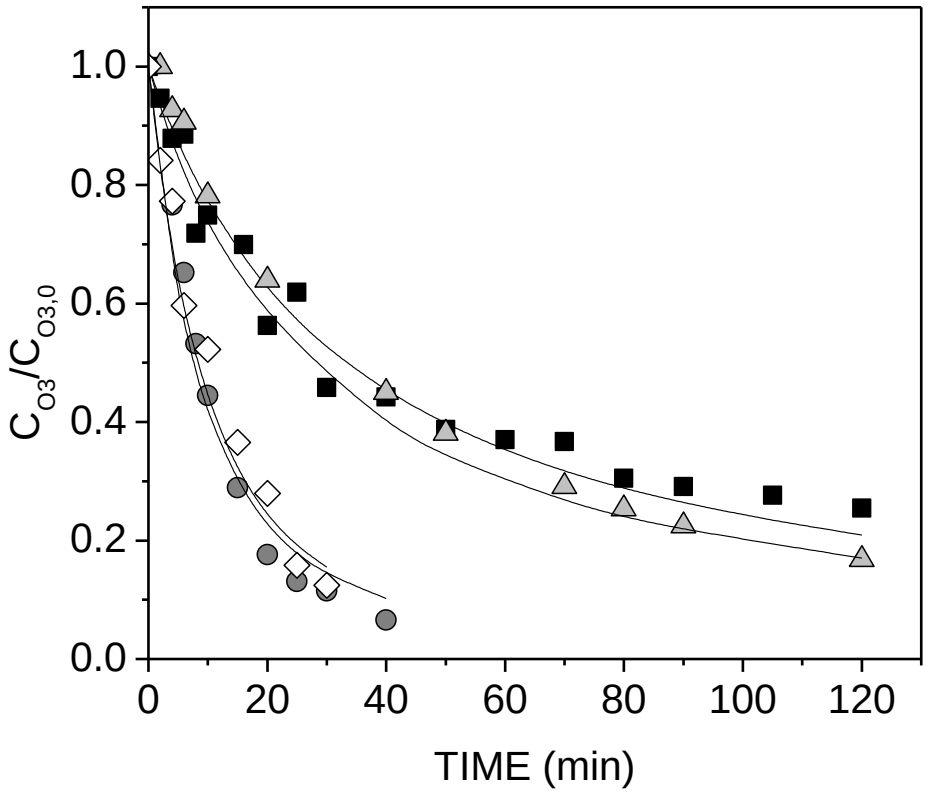

Fig. 6. Time-evolution of normalized aqueous ozone concentration during the course of batch ozone decomposition experiments. Experimental conditions: V=500 mL, pH=4 (10 mM phosphate buffer), $C_{O3,0}$=1.5x10^{-4} M, T=37ºC. Symbols*:* ■ No radiation, ● Radiation (λ=300-800 nm), filter A ◇ Radiation (λ=320-800 nm), filter A+B, △ Radiation (λ=390-800 nm), filter A+C. See Table 2 for irradiance distribution. Solid lines represents fitting results according to the model in Table 4.

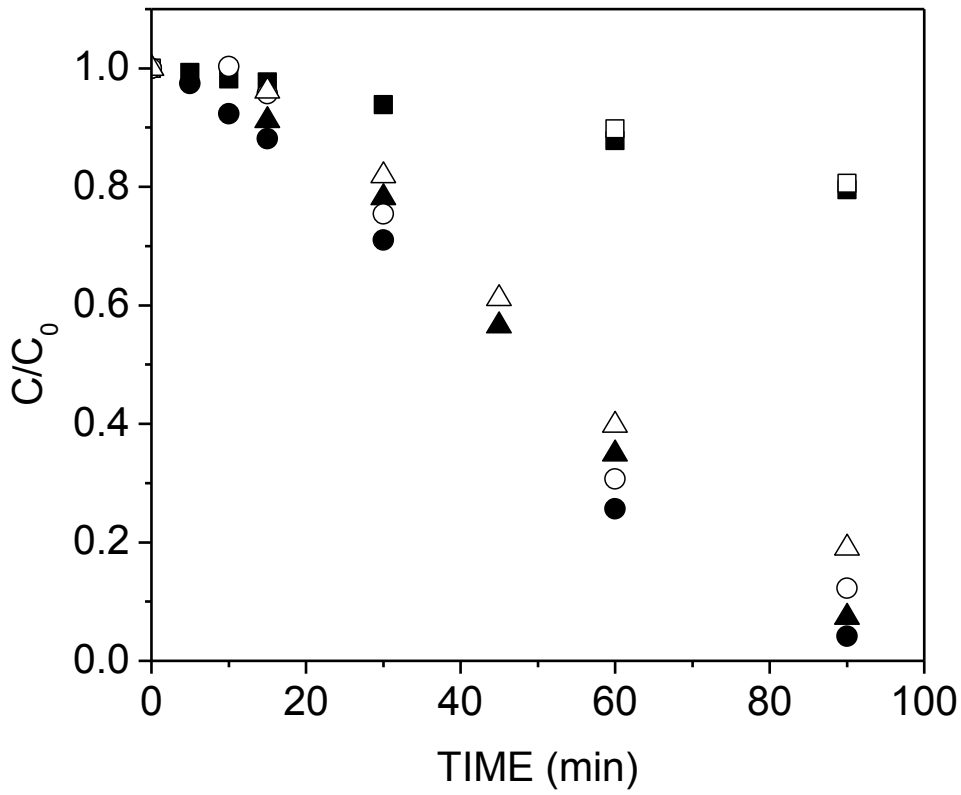

Fig. 7. Time-evolution of normalized oxalic acid concentration and normalized TOC during the course of semi-batch ozonation and photo-ozonation experiments. Experimental conditions: V=500 mL, $C_{OXAL,0}$=25 mg L^{-1}, pH_0=4, T=37ºC, Ozone dosage=2.5 mg min^{-1}. Symbols: ■, □ O_3; ●, ○ Photo-ozonation (λ>300 nm); ▲,△ Photo-ozonation (λ>320 nm). Solid symbols for oxalic acid, open symbols for TOC.

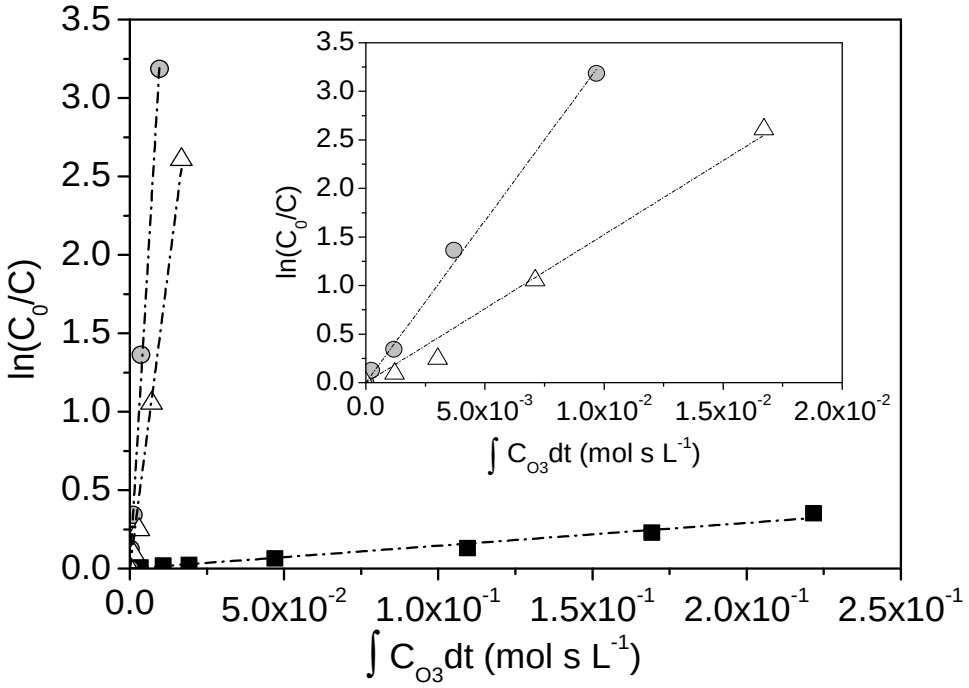

Fig. 8. R_{ct} plots for ozonation and photo-ozonation semi-batch experiments. Operating conditions: V=500 mL, $C_{OXAL,0}$=25 mg L^{-1}, pH_0=4, T=37ºC, Ozone dosage=2.5 mg min^{-1}. Symbols: ■ O_3, ● Photo-ozonation (λ>300 nm), △ Photo-ozonation (λ>320 nm).

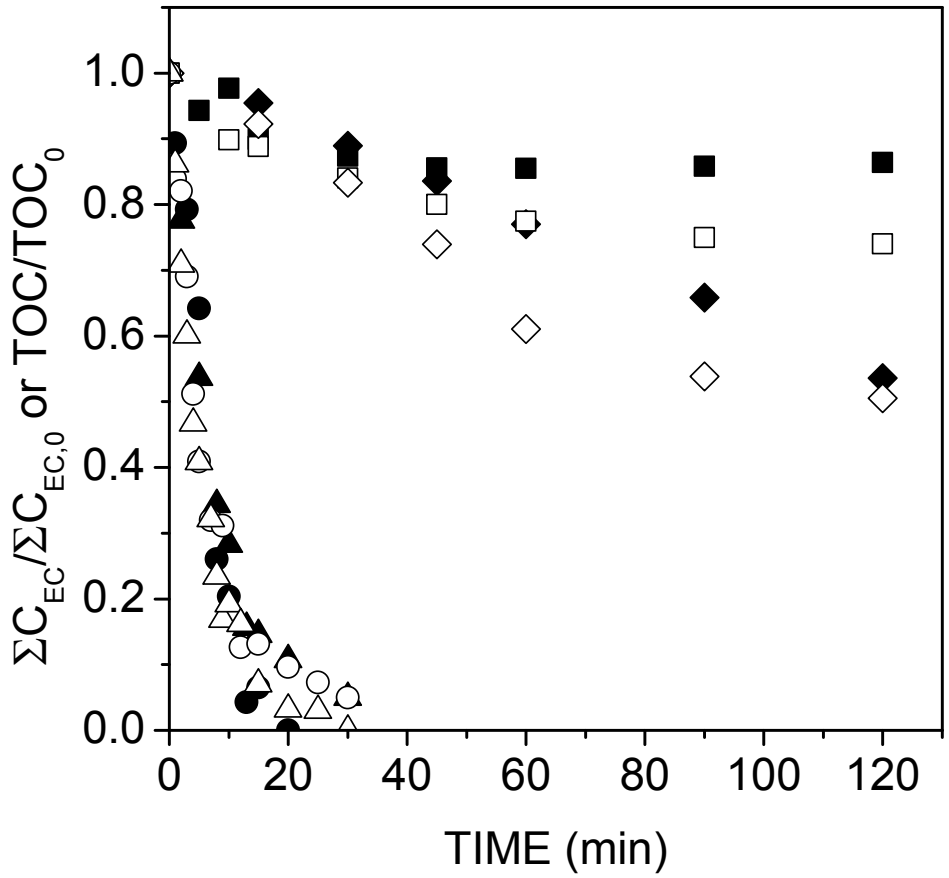

Fig. 9. Time-evolution of normalized overall ECs concentration and normalized TOC during the course of semi-batch ozonation and photo-ozonation (λ>320 nm) experiments. Experimental conditions: V=500 mL, $C_{EC,0}$=2 mg L^{-1} each, TOC_0= 4 mg·L^{-1} (ultrapure water spiked with ECs) or 20 mg·L^{-1} (synthetic effluent), pH_0=7, T=37ºC, Ozone dosage=3.3 mg min^{-1}. Symbols: ■ □ O_3, TOC profile; ●, ○ O_3, ECs concentration profile; ◆,◇ Photo-ozonation, TOC profile; ▲,△ Photo-ozonation, ECs concentration profile. Solid symbols for experiments with the synthetic effluent (see Table 1), open symbols for experiments carried out in ultrapure water spiked with ECs.

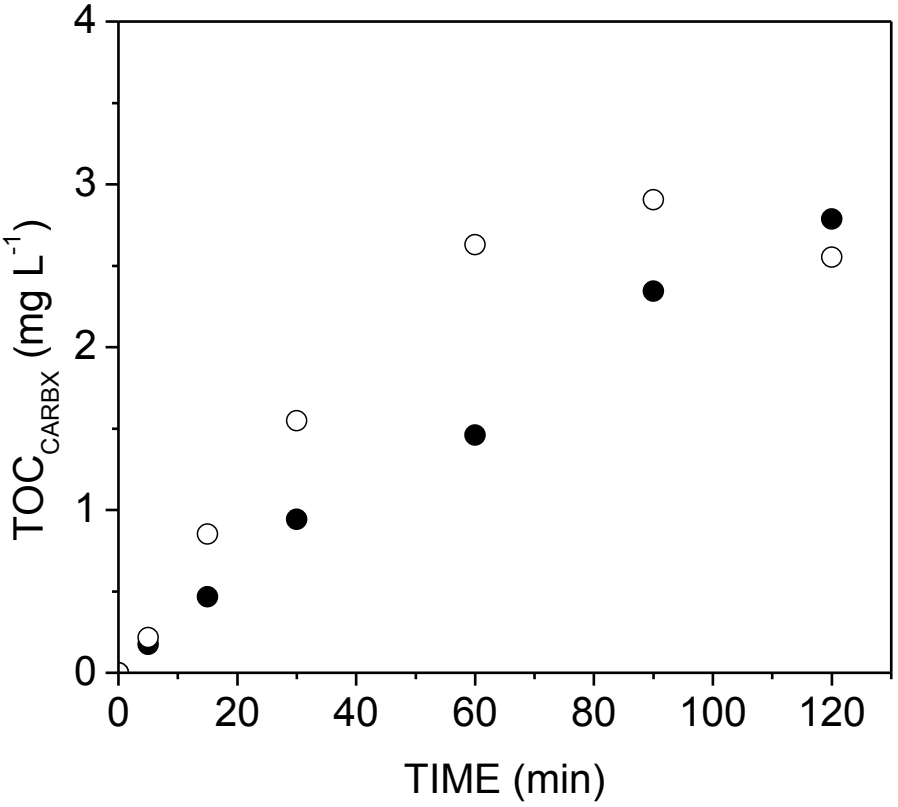

Fig. 10. Time-evolution of short-chain carboxylic acids (measured as organic carbon) accumulated during ozonation and photo-ozonation semi-batch experiments carried out with the synthetic effluent. Experimental conditions: V=500 mL, $C_{EC,0}$=2 mg L^{-1} each TOC_0=20 mg L^{-1}, pH_0=7, C_{O3ge}=10 mg L^{-1}, Q=20 L h^{-1}, T=37ºC, Ozone dosage=3.3 mg min^{-1}. Symbols: ● O_3, ○ Photo-ozonation (λ>300 nm).